Available online at www.sciencedirect.com
SCIENCE DIRECT
Journal of Catalysis 236 (2005) 34–44
JOURNAL OF CATALYSIS
www.elsevier.com/locate/jcat

# Effect of precipitate aging on the microstructural characteristics of Cu/ZnO catalysts for methanol steam reforming

B.L. Kniep, F. Girgsdies, T. Ressler *

*Department of Inorganic Chemistry, Fritz Haber Institute of the Max Planck Society, Faradayweg 4-6, 14195 Berlin, Germany*

Received 12 May 2005; revised 30 August 2005; accepted 1 September 2005

Available online 17 October 2005

**Abstract**

Microstructural characteristics of the copper phase in Cu/ZnO catalysts for methanol steam reforming (MSR) were investigated as a function of aging of the precipitated hydroxycarbonates during catalyst preparation. The bulk structure of active catalysts under MSR reaction conditions was determined by in situ X-ray diffraction (XRD) and in situ X-ray absorption spectroscopy (XAS) combined with on-line mass spectrometry. Reduction kinetics and phase compositions obtained from XAS data analysis were compared with conventional TPR and TG/MS results. With increasing aging time of the precipitate, the onset of reduction of the CuO/ZnO precursor shifted from 462 to 444 K, whereas a decrease in crystallite size from 110 Å (0 min) to 70 Å (120 min) was detected. A strong increase in catalytic activity was observed for Cu/ZnO catalysts obtained from precipitates aged for more than 30 min. The microstrain in the copper particles as detected by XRD and XAS was determined as an additional bulk structural parameter correlating with the increase in catalytic activity. Moreover, continuous precipitate aging led to a decreasing amount of Zn in the copper clusters of the Cu/ZnO catalysts. A schematic model of the structural characteristics of Cu/ZnO catalysts as a function of precipitate aging is proposed. This model emphasizes the defect-rich state of the homogeneous microstructure of Cu/ZnO catalysts and its implication for the catalytic activity in the steam reforming of methanol.


*Keywords:* Methanol; Steam reforming; Copper; Zinc oxide; Structure–activity relationship; Microstrain; Aging; Rational design; XAS; XRD

## 1. Introduction

$Cu/ZnO/Al_2O_3$ catalysts are industrially used for methanol synthesis and the water–gas shift reaction, and are also known to be active for the steam reforming of methanol ($CH_3OH + H_2O \rightarrow CO_2 + 3H_2$) [1]. To elucidate pathways to producing improved catalysts for methanol steam reforming, a fundamental understanding of the relation between surface structure, bulk structure, and catalytic activity is required. Along with previous investigations assuming a linear correlation between the copper surface area and the catalytic activity [2], recent investigations have shown that differently prepared Cu/ZnO catalysts may have differently active specific copper surfaces and thus exhibit additional microstructural factors contributing to the correlation between surface area and catalyst performance in methanol chemistry [3,4]. Klier proposed that $Cu^+$ species dissolved in ZnO enhance the catalytic activity for methanol synthesis [5]. Based on surface science investigations of model catalysts with Zn deposited on Cu(111) surfaces, Fujitani et al. [6] suggested that a metallic Cu–Zn surface alloy is the catalytically active species for methanol synthesis. In addition to an alloying effect, dynamical and reversible changes in the morphology of the Cu particles may be caused by changes in the reduction potential of the gas phase (wetting/nonwetting) [7,8]. An increase in oxidation potential results in spherical Cu particles on large crystals of ZnO (i.e., nonwetting), whereas a subsequent decrease of the oxidation potential results in disc-like Cu particles on ZnO (i.e., wetting). Furthermore, it is assumed that methanol synthesis activity is enhanced by hydrogen spillover from ZnO [9].

Recently, we showed that methanol synthesis and methanol steam-reforming activity of binary Cu/ZnO catalysts with varying molar ratios correlate with the microstrain in the copper particles [10,11]. Density functional theory calculations [12] indicate that strained copper surfaces can affect the catalytic activity because of changes in, for instance, adsorption energies and dis-

* Corresponding author. Fax: +49 30 8413 4405.
*E-mail address:* ressler@fhi-berlin.mpg.de (T. Ressler).

0021-9517/$ – see front matter 
doi:10.1016/j.jcat.2005.09.001

sociation barriers of hydrogen. Defects in the bulk structure, such as microstrain, impurities, and structural disorder, may significantly influence the performance of the corresponding copper catalyst. Hence, understanding the correlations between particular preparation parameters and the microstructure of the resulting catalyst are prerequisites for a knowledge-based catalyst design. Precipitation of mixed copper–zinc hydroxycarbonates is a common method of preparing highly active Cu/ZnO catalysts. Aging of freshly precipitated Cu–Zn hydroxycarbonates exhibits a strong influence on the catalytic properties of the resulting Cu/ZnO catalysts. Increased catalytic activity as a result of prolonged precipitate aging has been demonstrated for methanol synthesis, reverse water–gas shift reaction [13], CO oxidation [14–16], and the methanol steam-reforming reaction [17]. Thus aging permits improved catalyst performance by tailoring the preparation conditions instead of varying the chemical composition [17]. Previous investigations concerning structural changes of the precursors during aging in the mother liquor revealed that the initially amorphous precipitates (e.g., georgeite) transform after a certain time into a mixture of crystalline rosasite (zincian malachite) and aurichalcite [18]. Although changes in the morphology of the copper catalysts obtained from aged precursors have been investigated, [16] details of the bulk structure–activity relationship have not yet been fully identified. This work focuses on the correlation between the increased activity of copper catalysts prepared from aged precipitates and the structure of the copper phase of the active catalyst under working conditions. Complementary bulk methods are used to investigate the long-range order (i.e., in situ X-ray diffraction) and the short-range order (i.e., in situ X-ray absorption spectroscopy), in combination with on-line mass spectrometry. A structural model of the active catalyst as function of precipitate aging and its influence on the catalytic activity is proposed.

## 2. Experimental

### 2.1. Preparation

Copper zinc hydroxycarbonate precursors were prepared by co-precipitation [18]. Co-precipitation was performed in a reaction container filled with 400 ml of bidistilled water (353 K) by simultaneous mixing of an aqueous solution of metal nitrates ($Cu(NO_3)_2 \cdot 3H_2O$ and $Zn(NO_3)_2 \cdot 6H_2O$ (600 ml of a 1 M metal nitrate solution; molar ratio of copper to zinc of 70:30 in the nitrate solution) with sodium carbonate (1.2 M) at constant pH (pH 7). The nitrate solution was added at a constant rate of 25 ml/min. The addition rate of the precipitation reagent ($Na_2CO_3$) was controlled as described previously [18], to adjust the desired pH in the mother liquor. After complete addition of the solutions, the resulting precipitates were aged under continuous stirring in the mother liquor at 353 K for 15, 30, and 120 min. The differently aged suspensions were purged out of the reactor followed by separation of the precipitates from the mother liquor by vacuum filtration (for about 60 s). For the 0-min aged sample, the precipitate was filtered directly after complete addition of the nitrate and soda solutions. After filtering, half of the resulting filter cake (20 g) was washed six times with deionized water (80 ml) in a 250-ml beaker for 10 min under continuous stirring at 333 K. Finally, 3 g of the washed precipitate were dried at 393 K for 10 h in static air (three $Al_2O_3$ boats, 1 g precipitate each), followed by calcination at 603 K in static air for 3 h (6 K/min).

### 2.2. TG/MS

Thermogravimetric analysis was conducted during reduction on a NETSCH STA 499 C in a constant gas flow of a 2 vol% $H_2$ in helium at a total flow of 100 ml/min. Approximately 15 mg of each of the calcined precursors was heated in an $Al_2O_3$ crucible to 523 K with a heating ramp of 6 K/min. Evolution of gas phase composition during reduction was monitored with a quadropole mass spectrometer (Pfeiffer Omnistar).

### 2.3. Catalytic activity and copper surface area determination

Reduction of the CuO/ZnO precursors was performed in 2 vol% $H_2$ in the temperature range 300–523 K at a heating ramp rate of 6 K/min, followed by an isothermal period of 30 min at 523 K. For in situ XRD and in situ XAS experiments, the four Cu/ZnO samples obtained from the differently aged precursors were cooled to 298 K after reduction and exposed to the steam-reforming gas mixture using saturators for methanol and water (ratio $CH_3OH{:}H_2O = 1{:}1$; ∼2.5 vol% $CH_3OH$/2.5 vol% $H_2O$/95 vol% He) at atmospheric pressure. The temperature was increased from 298 to 523 K at a ramp rate of 6 K/min at a total flow of 160 ml/min in the in situ XRD cell and 40 ml/min in the in situ XAS cell. Evolution of the gas phase composition was monitored with a mass spectrometer (Pfeiffer Omnistar). A total of 13 mg of the catalyst sample was used for the XRD experiments; 3 mg catalyst diluted in 30 mg BN was used for the XAS experiments. The methanol steam-reforming activity (i.e., hydrogen production rate) was calculated under isothermal conditions (523 K) at steady state (after ∼30 min). The methanol conversion in the XAS cell amounted to ∼10%. All Cu/ZnO catalysts studied exhibited a spiked increase in activity followed by a decrease in activity of approximately 5% of the maximum value in a 30-min period.

Catalytic activity determined in the in situ experiments was compared with activity measurements of the catalyst in a tubular stainless steel reactor placed in an aluminum-heating block. For these measurements, the catalyst powder was diluted with BN and pressed into pellets. Subsequently, these pellets were ground and sieved to obtain a defined particle size. The methanol conversion of the four catalysts obtained from differently aged precursors was determined at 523 K using a Varian 3800 gas chromatograph. More details on the experimental conditions used have been given elsewhere [19].

The specific copper surface area was determined by $N_2O$ decomposition ($N_2O + 2Cu_s \rightarrow N_2 + Cu_s{-}O{-}Cu_s$) [20,21] ($T = 313$ K, 0.5 vol% $N_2O$ in helium, Cu surface atom density $1.47 \times 10^{19}$ $m^{-2}$ [22]). 50 mg of the catalyst diluted in 50 mg BN was placed on a quartz frit in a quartz tube reactor (bed

height of about 15 mm). The temperature was measured by a thermocouple positioned in the powder bed. Before surface area was determined, the sample was reduced in 2 vol% $H_2$ (total flow of 40 ml/min) at 523 K according to the procedure described above. After reduction, the sample was cooled to 313 K, and the reactor was purged with He for 1 h. The Cu surface area was determined by monitoring the ion current of $m/e = 44$ (i.e., $N_2O$) using a mass spectrometer. More details on the method used have been given elsewhere [23].

### 2.4. Temperature-programmed reduction

Temperature-programmed reduction (TPR) was performed using a Thermoquest TPD/R/O 1100 instrument [5% $H_2$ in Ar (40 ml/min), at heating ramp rate of 6 K/min to 523 K followed by an isothermal period of 1 h at 523 K]. Here 20 mg of the catalyst powder was diluted in 250 mg of silicon carbide (115 mesh) and placed in the reactor (bed height of about 4 mm). Before the measurement, the sample was heated in Ar (20 ml/min) to 423 K (10 K/min), followed by an isothermal period of 30 min at 423 K.

### 2.5. In situ X-ray diffraction

In situ X-ray powder diffraction experiments were performed using a STOE Bragg-Brentano diffractometer (Cu-$K_\alpha$ radiation, secondary monochromator, scintillation counter). Reduction of the calcined CuO/ZnO precursors was carried out in an in situ cell (Bühler HDK S1) as described above. XRD patterns were recorded at 523 K under methanol steam-reforming conditions in a $2\theta$ range from 28.0° to 93.0° with a step width of 0.04° (counting time, 2 s/step). A sum of pseudo-Voigt profile functions and an appropriate background function were refined to the in situ XRD patterns of the Cu/ZnO catalysts according to the Pawley method (i.e., "full pattern refinement"). Lattice constants of Cu and ZnO, a linear zero shift in the $2\theta$ scale, four coefficients of the background polynomial, peak intensity, and the Gaussian and Lorentzian parts of the pseudo-Voigt profile of each individual hkl line were allowed to vary in the refinement. The volume-averaged copper crystallite size (diameter) and microstrain were determined from the Lorentzian and Gaussian parts of the individual profile functions [24]. An alternative method for determining crystallite size and microstrain by analyzing X-ray diffraction line profiles has been described by Williamson and Hall [25]. However, an isotropic distribution of both size and strain is a prerequisite for a linear correlation between $d^* = 2\sin\theta/\lambda$ and $\beta^* = \beta\cos\theta/\lambda$ and the applicability of the Williamson–Hall analysis.

### 2.6. In situ X-ray absorption spectroscopy

In situ XAS experiments were performed in a flow reactor in transmission geometry at the Cu $K$-edge ($E = 8.979$ keV) at the Hamburger Synchrotron Radiation Laboratory (HASYLAB; beamlines E4 and X1). The CuO/ZnO precursors were diluted in boron nitride and pressed for 1 min at 1.5 t into 5-mm-diameter pellets. Reduction of the precursors was performed as described above. Time-resolved X-ray absorption near-edge structure (XANES) measurements at the copper $K$-edge (time resolution = 100 s/spectrum; energy range, 8.9–9.1 keV) were done to determine phase composition and kinetics during reduction. The number of reference spectra required to reconstruct the set of experimental XANES spectra was obtained by a principle component analysis (PCA) [26,27]. The fraction of the reference spectra in each XANES spectrum was determined by a least squares fit of a linear combination of the reference spectra to the experimental spectra.

After reduction of the CuO/ZnO precursor, the extended X-ray absorption fine structure (EXAFS) of the resulting Cu/ZnO catalyst was measured under methanol steam-reforming conditions at 523 K. A copper foil was used as reference for energy calibration. Two polynomials were used for background subtraction and normalization, and the atomic background in the EXAFS region was determined by cubic splines. The radial distribution function was obtained by Fourier transformation of the $k^3$-weighted experimental spectrum $\chi(k)$ ($k$ range, 2.3–11.5 Å$^{-1}$) in the $R$ space. Multiple and single scattering paths in an fcc Cu model structure were calculated using FEFF 8 [28] in a range of 1.5–6.0 Å (5% lower limit with respect to the strongest scattering path). Refinement of the Cu model structure to the experimental EXAFS spectrum was carried out in $R$ space. Structural parameters refined include the single scattering shell distances ($R$), the Debye–Waller factors of the single scattering paths ($\sigma^2$), and one $E_0$ shift for all scattering paths. The coordination numbers (CNs) were kept constant because of the rather large Cu crystallite sizes (>70 Å). In addition, refinement of the Debye–Waller factor of a particular multiple scattering path was used as an indicator for structural disorder (i.e., strain). This particular scattering path corresponds to a linear arrangement of backscatterers in the Cu fcc structure. Because of the so-called "focusing effect," this path exhibits an exceptionally high contribution to the overall pseudoradial distribution function, $FT(\chi(k)^*k^3)$, and is particularly susceptible to deviations from a linear arrangement (i.e., disorder and strain).

## 3. Results

### 3.1. Characterization of the calcined CuO/ZnO precursors

Fig. 1a shows the CuO crystallite size of the calcined precursors (CuO/ZnO) in comparison with the Cu particle size of the reduced Cu/ZnO catalyst determined by line profile analysis of XRD patterns of the precursors and the reduced Cu/ZnO catalysts. A strong decrease in CuO crystallite size can be seen for the precursors obtained from crystalline precipitates (30 and 120 min aging) compared with the precursors obtained from amorphous precipitates (0 and 15 min aging). Deviations in the lattice constants of CuO obtained by XRD refinement of a CuO model structure (ICDD-PDF-2: 5-661) to the experimental patterns of the CuO/ZnO precursors are depicted in Fig. 1b. The lattice constants determined for the CuO/ZnO precursors obtained from precipitates aged for 0 and 15 min deviate significantly from those of ideal CuO. Conversely, only minor

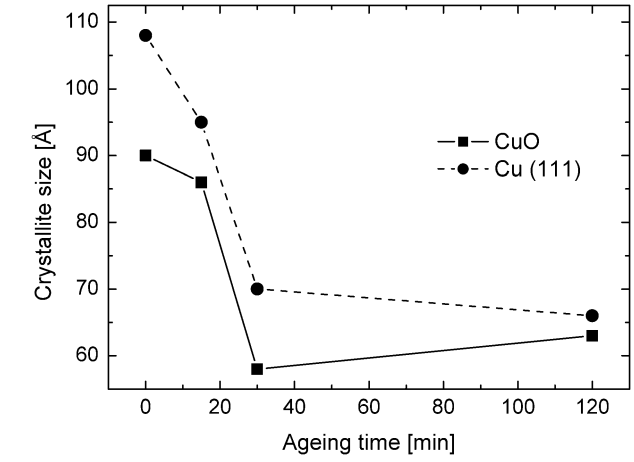


(a)

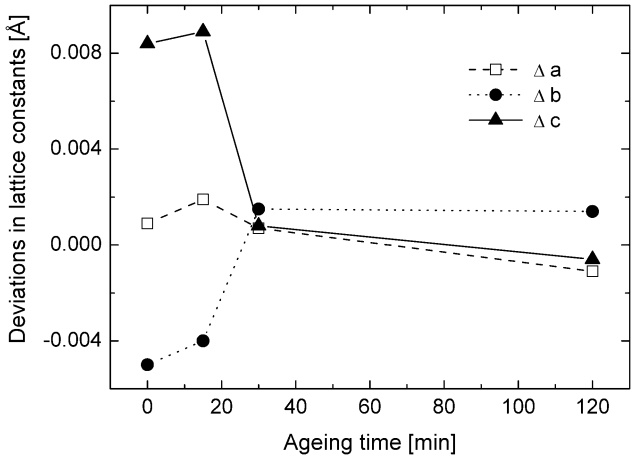


(b)

Fig. 1. (a) Crystallite size of CuO in CuO/ZnO precursors and of Cu in the reduced Cu/ZnO catalysts as function of precipitate ageing determined from XRD line broadening. (b) Deviations in the lattice constants of CuO in CuO/ZnO precursors as function of precipitate ageing.

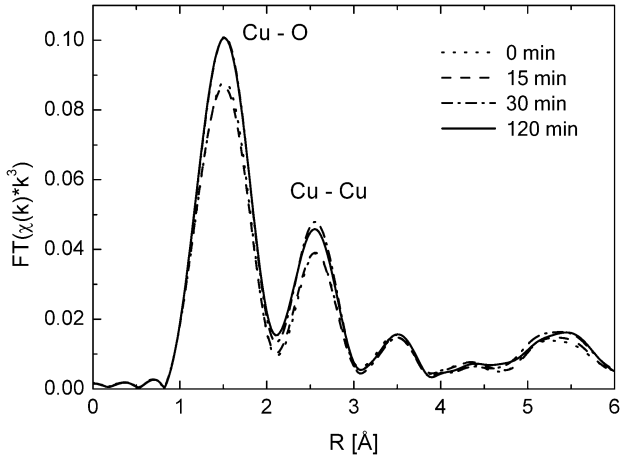


Fig. 2. Experimental Cu $K$-edge $FT(\chi(k)^*k^3)$ of CuO/ZnO precursors obtained from precipitates aged for 0, 15, 30, and 120 min.

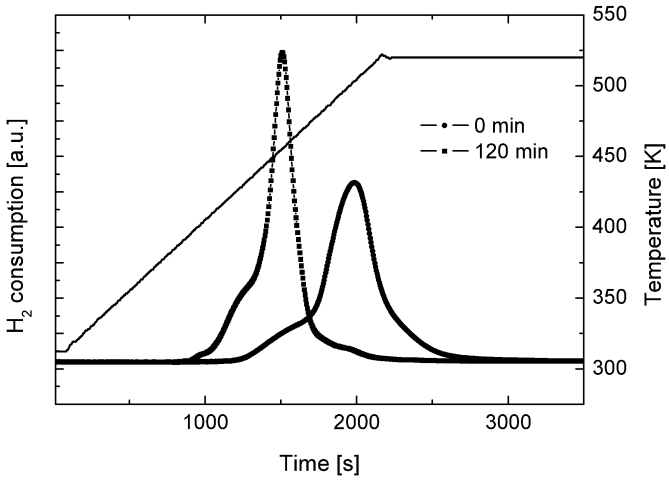


Fig. 3. Hydrogen consumption during temperature-programmed reduction (TPR) of two CuO/ZnO precursors (0 and 120 min ageing) in the temperature range from 300 to 523 K (heating ramp 6 K/min).

deviations in the lattice constants of CuO were observed for the CuO/ZnO precursors obtained from precipitates aged for 30 and 120 min. The distinct distortion of the CuO short-range structure of the CuO/ZnO precursors obtained from precipitates aged for 0 and 15 min is also visible in the Cu $K$-edge $FT(\chi(k)^*k^3)$ (Fig. 2). The first peak in the $FT(\chi(k)^*k^3)$, attributed to Cu surrounded by oxygen in a square-planar coordination, and the second peak, attributed to the first Cu shell in CuO, exhibit a strongly decreased intensity for the precursors obtained from precipitates aged for 0 and 15 min.

### 3.2. Reduction of the CuO/ZnO precursor

The consumption of hydrogen during TPR of two CuO/ZnO precursors (0 and 120 min aging) in the temperature range 300–523 K are depicted in Fig. 3. Both TPR traces exhibited characteristic shoulders left to the main reduction peak. Compared with the narrow reduction peak at 454 K of the CuO/ZnO precursor obtained from a 120-min aged precipitate, the TPR traces of the CuO/ZnO precursor obtained from a nonaged precipitate were much broader and shifted to higher reduction temperatures (503 K). The onset temperature of reduction and the shape of the TPR traces of the CuO/ZnO precursor obtained from precipitates aged for 15 and 30 min are in good agreement with the TPR traces of the precursors aged for 0 and 120 min, respectively. PCA of time-resolved XANES spectra measured during reduction yielded three reference compounds (CuO, $Cu_2O$, and Cu) required for reconstructing the set of experimental XANES spectra. Target-transformed XANES spectra of CuO and Cu are in good agreement with the first and last experimental spectra. Differences between the Cu $K$-edge spectrum of crystalline $Cu_2O$ and the corresponding target-transformed spectrum can be attributed to a different crystallite size and the high disorder of the $Cu_2O$ formed during reduction. A quantitative phase analysis was obtained from a least squares fit of a linear combination of the Cu and CuO reference spectra and the target-transformed spectra of $Cu_2O$ to each experimental XANES spectrum measured during reduction of the CuO/ZnO precursor. The resulting evolution of the phase composition during reduction of CuO/ZnO (15 min aging) and the

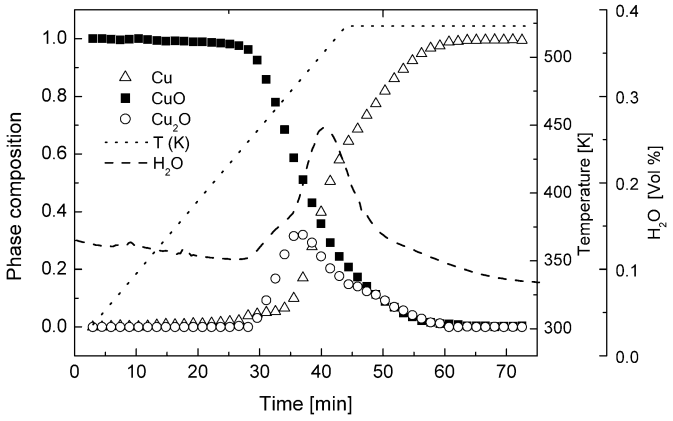


Fig. 4. Evolution of phase composition (CuO, $Cu_2O$, and Cu) and $H_2O$ signal during temperature-programmed reduction of a CuO/ZnO precursor (15 min aged precipitate) in 2% $H_2$ (300 to 523 K; 6 K/min) obtained from time-resolved Cu $K$-edge XANES measurements.

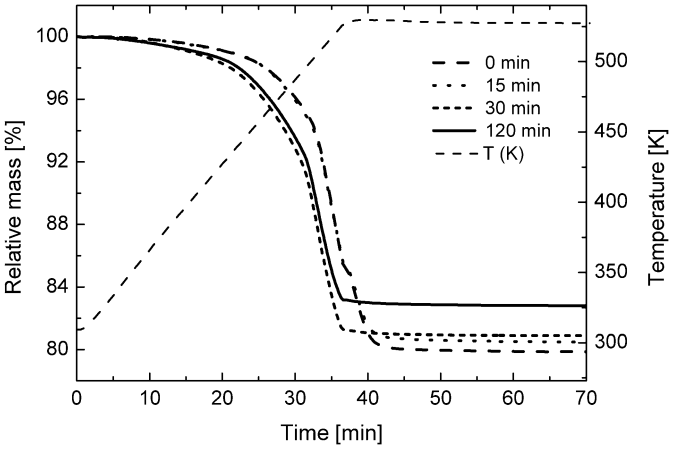


Fig. 5. Evolution of relative weight during temperature-programmed reduction of CuO/ZnO precursors obtained from differently aged precipitates (0, 15, 30, and 120 min) (2% $H_2$, 300 K to 523 K; 6 K/min).

corresponding $H_2O$ evolution are shown in Fig. 4. A sequential reduction pathway from CuO to intermediate $Cu_2O$ and, eventually, to Cu metal was found, in good agreement with previous investigations [10,11].

The evolution of the relative mass of the four CuO/ZnO precursors during TPR is depicted in Fig. 5. The difference in the mass loss after reduction of the CuO/ZnO precursors obtained from precipitates aged for 120 and 0 min resulted from the different composition of the materials. A quantitative determination of the Cu content in the catalyst obtained from the copper $K$-edge jump and zinc $K$-edge jump exhibited a decrease in copper content from 75 mol% (0 min aging) to 73 mol% copper (120 min aging) with respect to the metals. Moreover, different amounts of residual nitrates and carbonates remained in the CuO/ZnO precursors after preparation. The evolution of the gas phase composition during TPR of CuO/ZnO obtained from precursors aged for <30 min clearly indicates the decomposition of residual nitrates (NO, $m/e = 30$) and carbonates ($CO_2$, $m/e = 44$). The amount of residual carbonates and nitrates in the precursors decreased with increasing aging time. Residual copper oxide phases indicating an incomplete reduction of the CuO/ZnO precursors were not detected (detection limit of XAFS analysis, ∼1%).

### 3.3. Methanol steam reforming on Cu/ZnO catalysts

The $H_2$ production rate during methanol steam reforming on the Cu/ZnO catalysts as determined in the in situ XAS cell and the methanol conversion as determined in the tubular reactor as a function of aging time are compared in Fig. 6. The activity of the Cu/ZnO catalysts in the tubular reactor strongly increased between 15 and 30 min aging time from an initial 36% methanol conversion (XAS cell: 600 µmol/(g s) $H_2$ production rate, 15 min aging) to 60% conversion (XAS cell: 900 µmol/(g s) $H_2$ production rate, 30 min aging). A similar dependence of the methanol steam-reforming activity of the Cu/ZnO catalysts on the aging time was found for the in situ XRD experiments. The good agreement between the catalytic performance measured in the in situ XAS cell and the steel reactor (Fig. 6) indicates that the structural data obtained from in situ XAS experiments under conditions of differential conversion (∼10% methanol conversion in the XAS cell) enable deduction of reliable structure–activity relationships.

Fig. 7 compares the specific copper surface areas as determined by $N_2O$ decomposition with those calculated from the respective volume-averaged copper crystallite size (i.e., diameter, XRD) assuming spherical crystallites. An increasing aging time resulted in an increase in the Cu surface area from initially 13 $m^2/g_{cat}$ after 0 min aging (20 $m^2/g_{cat}$ by XRD) to 21 $m^2/g_{cat}$ after 120 min aging (33 $m^2/g_{cat}$ by XRD). Both methods revealed similar trends in the evolution of the Cu surface area as a function of precipitate aging. Cu/ZnO support interactions that reduce the accessible Cu surface area and a nonspherical morphology of the Cu particles may account for the deviations in the Cu surface areas obtained, in addition to a bimodal particle size distribution or reoxidation of partially reduced ZnO. The normalized $H_2$ production rates measured during the in situ XAS measurements as a function of the spe-

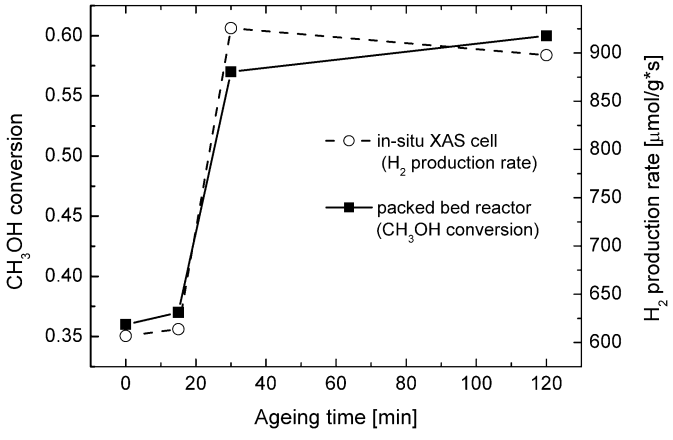


Fig. 6. Methanol steam reforming activity of Cu/ZnO catalysts at 523 K as a function of precipitate ageing. The methanol conversion determined in a packed bed reactor is depicted in comparison to the $H_2$ production rate obtained during the in situ XAS experiment.

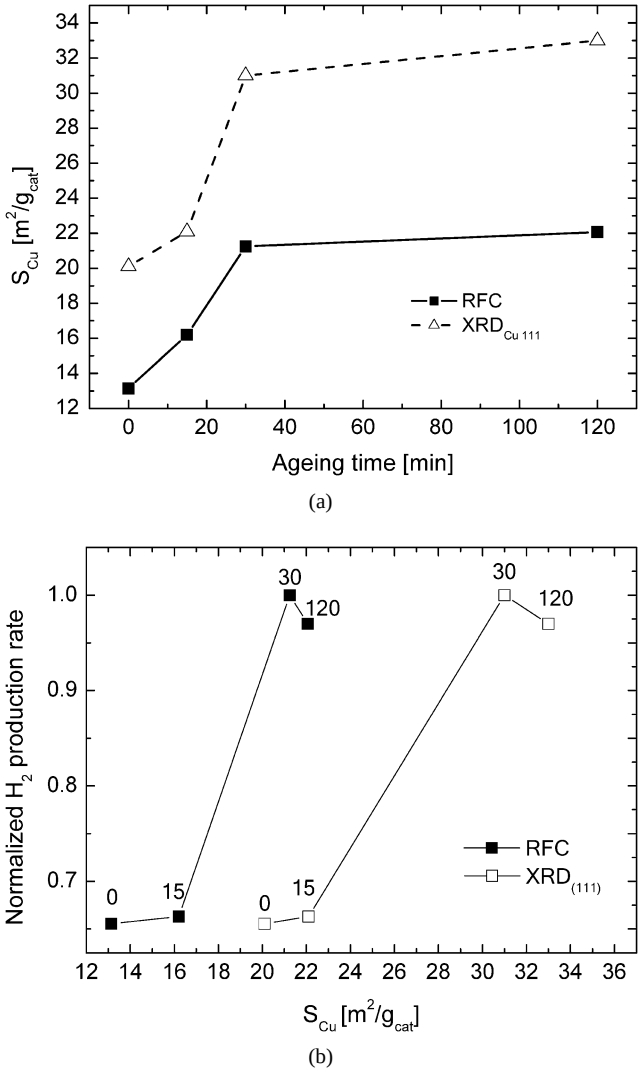


Fig. 7. (a) Specific copper surface area of Cu/ZnO catalysts as a function of precursor ageing determined by $N_2O$ titration and estimated from the XRD copper particle size (Fig. 8, Cu 111). (b) Normalized $H_2$ production rate according to Fig. 6 as a function of the specific copper surface area.

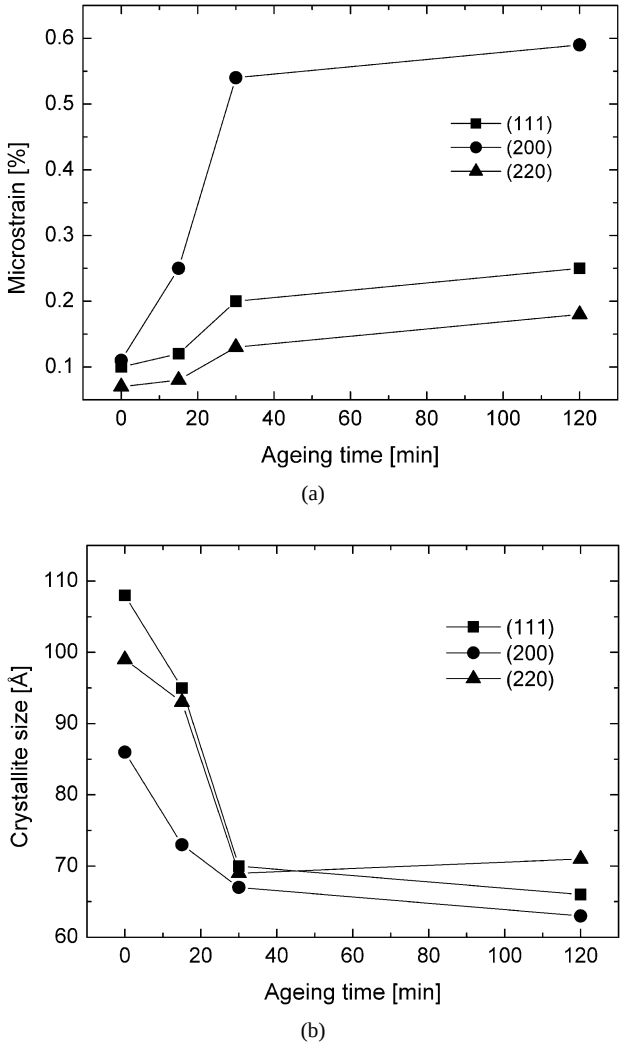


Fig. 8. (a) Copper microstrain (b) and crystallite size as function of precipitate ageing determined from the Cu (111), (200), and (220) XRD lines of Cu/ZnO catalysts under methanol steam reforming conditions at 523 K.

cific Cu surface area are depicted in Fig. 7b. The $H_2$ production rate is normalized to the activity of the most active catalyst in the steam reforming of methanol (30 min aging).

### 3.4. Long-range order from in situ X-ray diffraction

Quantitative phase analysis of the in situ XRD patterns of the reduced Cu/ZnO catalysts (at 0, 15, 30, and 120 min) measured under steam-reforming conditions at 523 K revealed a phase composition of 68 mol% copper and 32 mol% zinc oxide [17]. Although the phase compositions of the four Cu/ZnO catalysts were very similar, the profiles of the individual copper diffraction lines in the patterns of the catalysts exhibited significant differences. Analysis of the Cu (111) line profile as a function of precipitate aging revealed a decrease of the copper crystallite size from the initial 110 Å (0 min aging) to 70 Å (120 min aging) (Fig. 8b), accompanied by an increase in copper microstrain from the initial 0.09% (0 min aging) to 0.25% (120 min aging) (Fig. 8a) [17]. In comparison, copper particles obtained from the reduction of CuO [obtained by calcination of malachite, $Cu_2(OH)_2(CO_3)$] exhibited a particle size of 300 Å and a microstrain of 0.06%.

Crystallite size and microstrain obtained from the analysis of three different copper diffraction lines (111, 200, 220) as function of precipitate aging are shown in Fig. 8. Distinct deviations in both crystallite size and microstrain obtained from different copper lattice planes can be seen. The Cu/ZnO samples analyzed here exhibited a preferred orientation in the [111] direction and a maximum microstrain in the [100] direction. Nevertheless, decreased crystallite size and increased microstrain as functions of precipitate aging were observed for all individual copper diffraction lines. A Williamson–Hall plot based on the XRD patterns of the four Cu/ZnO catalysts confirmed the strong anisotropy (i.e., nonlinearity between $\beta^*$ and $d^*$) in the Cu/ZnO catalysts shown in Fig. 8. Hence crystallite size and microstrain had to be determined by analyzing individual X-ray diffraction lines.

### 3.5. Short-range order from in situ X-ray absorption spectroscopy

X-Ray absorption spectra of the Cu/ZnO catalysts were measured at the Cu $K$-edge under methanol steam-reforming reaction conditions at 523 K. The resulting pseudoradial distribution functions [$FT(\chi(k)^*k^3)$] of the four Cu/ZnO catalysts obtained from differently aged precipitates are compared in Fig. 9. The $FT(\chi(k)^*k^3)$ of the catalysts were very similar above 3 Å, whereas the peak at $R = 2.2$ Å (not phase-shift corrected), which is attributed to the first Cu–Cu distance in fcc copper metal, exhibited a strong increase in amplitude with increasing aging time.

The results of a refinement of the Cu fcc model structure to the experimental Cu $FT(\chi(k)^*k^3)$ of a Cu/ZnO catalyst (120 min aging), together with the linear focusing multiple scattering paths, are shown in Fig. 10. The good agreement between theory and experiment indicates that no additional phases (e.g., copper oxides) were detectable in the EXAFS spectrum. The Debye–Waller factor of the multiple scattering path used to estimate the amount of microstrain in the Cu/ZnO catalysts is given in Fig. 11. An increase in the Debye–Waller factor with aging time was detected. Conversely, the simultaneous decrease of the amount of Zn in the copper phase should yield a decrease in the Debye–Waller factor (i.e., an increase in amplitude), as was seen in the first Cu shell of the corresponding Cu/ZnO catalysts (Fig. 9). Therefore, the behavior of the particular "focusing" multiple scattering path as a probe for microstrain in the copper phase is in good agreement with the increase in microstrain as a function of precipitate aging as obtained by XRD line profile analysis.

In addition, the distances of the first Cu shell in the four $FT(\chi(k)^*k^3)$ of the Cu/ZnO catalysts were obtained from the EXAFS analysis. Fig. 12 shows the evolution of the deviations in the distance of the first Cu shell (relative to $a = 3.615$ Å for bulk fcc copper metal) compared with the copper lattice

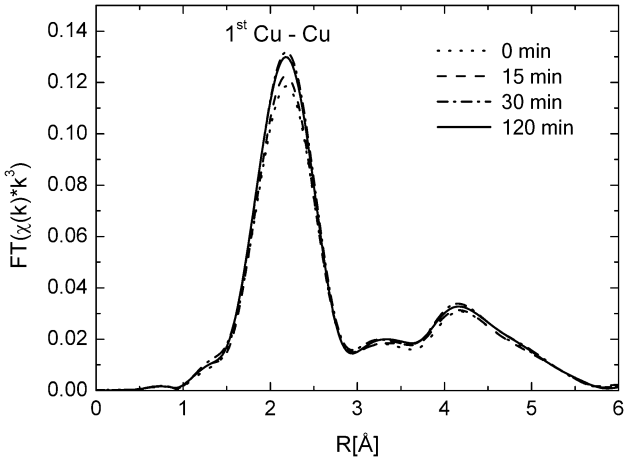


Fig. 9. Experimental Cu $K$-edge $FT(\chi(k)^*k^3)$ of Cu/ZnO catalysts obtained from precipitates aged for 0, 15, 30, and 120 min under methanol steam reforming conditions at 523 K.

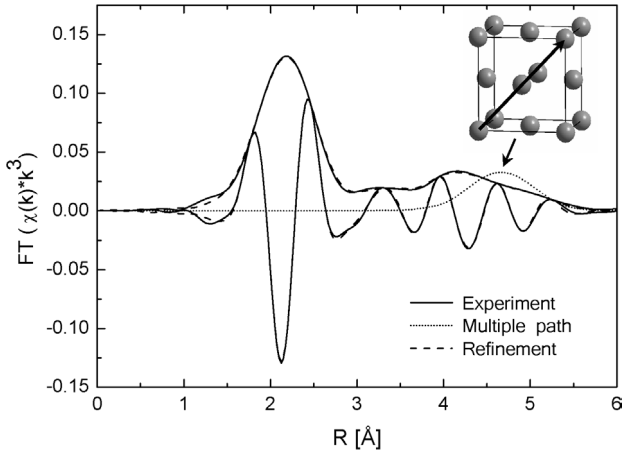


Fig. 10. Refinement of a theoretical EXAFS function (dashed) to the experimental Cu $K$-edge $FT(\chi(k)^*k^3)$ (solid) of a Cu/ZnO catalyst (120 min ageing) under methanol steam reforming conditions at 523 K. The four most prominent single-scattering paths (dotted) in the EXAFS function together with one multiple-scattering path (arrow in unit cell) are depicted.

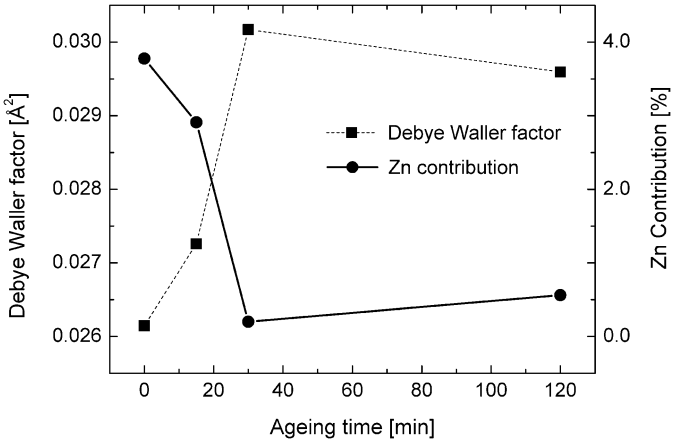


Fig. 11. Debye–Waller factors of the multiple-scattering path indicated by the arrow in Fig. 10 as function of precipitate ageing obtained by refinement of a theoretical Cu EXAFS function to the experimental $FT(\chi(k)^*k^3)$ of four Cu/ZnO catalysts (0, 15, 30, and 120 min ageing) measured at 523 K together with (b) the contribution of a Cu–Zn shell to the Cu $K$-edge $FT(\chi(k)^*k^3)$ of the Cu/ZnO catalysts as function of precipitate ageing.

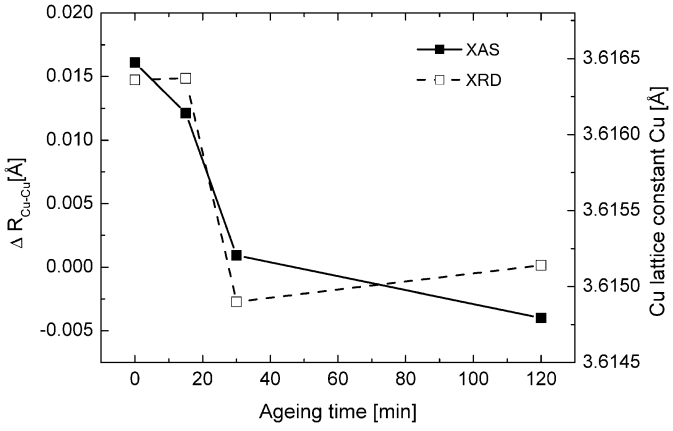


Fig. 12. Variation of the Cu lattice parameter determined by XRD under methanol steam reforming conditions at 523 K and deviations in the distance of the first Cu shell obtained from an EXAFS refinement to the experimental Cu $K$-edge $FT(\chi(k)^*k^3)$ as a function of precipitate ageing.

constants determined by XRD refinement. The decrease in the distance of the first Cu shell coincides with the decrease in copper lattice constant with aging time. The lattice expansion of the Cu crystallites in the Cu/ZnO catalysts obtained from precipitates aged for 0 and 15 min may indicate Zn occupying copper lattice sites, as was previously observed in Cu/ZnO catalysts with varying molar ratios [11]. To quantify the amount of Zn in the Cu nanoparticles, an additional Zn shell at a Cu–Zn distance of 2.66 Å [8] was included in the EXAFS refinement. The distances of the Cu–Cu and the Cu–Zn scattering paths were kept constant, whereas the sum of the coordination numbers of the Cu–Cu and Cu–Zn scattering paths was constrained to be 12 in the refinement. The amount of Zn scatterers necessary to simulate the first shell of the experimental spectra of the four Cu/ZnO catalysts is shown in Fig. 11, indicating a decreasing amount of Zn occupying Cu lattice sites in the catalysts obtained from precipitates aged for 30 and 120 min. The increased Cu–Cu distance of ∼0.016 Å in the Cu/ZnO catalysts obtained from short-aged precipitates is about one order of magnitude larger than the corresponding lattice expansion of 0.0014 Å as detected by XRD. This discrepancy may be accounted for by the XAFS refinement procedure used, which considers an average of the Cu–Cu distance ($R_{\mathrm{Cu–Cu}} = 2.55$ Å) and the Cu–Zn distance ($R_{\mathrm{Cu–Zn}} = 2.66$ Å) in the first shell. This may result in larger distance deviations in the short-range order than in the long-range lattice expansion as determined by XRD.

## 4. Discussion

### 4.1. Structure of the CuO/ZnO precursors

The long-range (Fig. 1) and short-range (Fig. 2) structures of the four CuO/ZnO precursors exhibited a characteristic dependence on the crystallization of the initially amorphous precipitates occurring after about 30 min aging [18]. The decrease in the CuO crystallite size of the calcined CuO/ZnO precursor with increasing aging time coincides with the decreasing Cu crystallite size of the reduced Cu/ZnO catalysts (Fig. 1a). Moreover, the CuO lattice constants of CuO/ZnO precursors obtained from precipitates aged for 30 or 120 min showed a remarkable shift toward those of regular CuO (Fig. 1b). The deviations in the CuO lattice constants of CuO/ZnO precursors obtained from short-aged precipitates (0 and 15 min) can be assigned to the formation of a Zn-doped CuO ($Cu_{1-x}Zn_xO$) [29,30].

The deviations in the short-range order structure of the CuO/ZnO precursors obtained from short-aged and long-aged precipitates are in good agreement with the corresponding long-range order structure of the materials (Fig. 2). The first peak in the XAFS $FT(\chi(k)^*k^3)$, corresponding to four oxygen atoms in a square-planar coordination, and the second peak, corresponding to the first Cu shell in CuO (Fig. 2), exhibited a strong increase in intensity for the precursors obtained from precipitates aged for 30 and 120 min. A similar increase was also visible in the $FT(\chi(k)^*k^3)$ of the corresponding reduced Cu/ZnO catalysts (Fig. 9). The increase in $FT(\chi(k)^*k^3)$ amplitude of the CuO/ZnO precursor and the Cu/ZnO catalysts may be explained by (i) an unlikely decrease in the Debye–Waller factor, which (at least for the Cu/ZnO catalysts) is in contrast to the increase in microstrain detected by XRD and NMR [17]; (ii) an increase in the apparent coordination number because of changes in crystallite size, which can be excluded because of the rather large crystallites (>70 Å [31]) and the overall decrease in crystallite size with aging; or, most likely, (iii) a decreasing amount of Zn in the CuO phase and the resulting copper catalyst. Hence it may be concluded that the deviations in the "real" structure of CuO in the calcined precursors obtained from short-aged precipitates (Figs. 1b and 2) are caused by Zn centers in the CuO structure. Similarly, Zn in the calcined CuO/ZnO precursors has been proposed for Cu/ZnO catalysts with various Cu/Zn ratios [10].

### 4.2. Reduction of the CuO/ZnO precursors

The four CuO/ZnO precursors studied can be separated into two groups with respect to the onset temperature of reduction (Figs. 3 and 5). CuO/ZnO precursors obtained from precipitates aged for 0 and 15 min exhibited a higher onset of reduction (∼450 K) compared with precursors obtained from precipitates aged for 30 and 120 min (∼500 K). The lower reduction temperature of the precursors obtained from long-aged precipitates compared with those obtained from short-aged precipitates results from the smaller CuO crystallite size (∼60 and ∼90 Å, respectively; Fig. 1a), the greater amount of strain and disorder, and the more homogeneous microstructure [32]. The increase in crystallite size during reduction of the nonaged CuO/ZnO precursor (∼90 Å) to the corresponding Cu/ZnO catalyst (∼110 Å) indicates a pronounced sintering of the copper particles. Similar to the increased onset of reduction, this lowered stability toward sintering is consistent with the larger amount of isolated copper particles and the diminished interface between Cu and ZnO in the catalysts obtained from short-aged precipitates [32]. Conversely, the more homogeneous particle size distribution and the improved interface between copper and zinc oxide in the Cu/ZnO catalysts obtained from long-aged precipitates increase the degree of dispersion and prevent sintering of the copper particles during reduction (∼65 Å for Cu and CuO) (Fig. 1a).

A quantitative XANES analysis (Fig. 4) allows assignment of a sequential reduction pathway to the two peaks observed during TPR (Fig. 3) according to $CuO \rightarrow Cu_2O \rightarrow Cu$. This is in good agreement with previous reports on the reduction of CuO in the $CuO/ZnO/ZrO_2$ system [33] and the reduction of CuO and $Cu_2O$ in $H_2$ [34]. Furthermore, it can be seen that the $H_2O$ evolution measured during the in situ XAFS experiments correlates with the phase composition during reduction (Fig. 4) and with the TPR measurements (Fig. 3). The first maximum in $H_2O$ evolution indicates the formation of intermediate $Cu_2O$, whereas the second maximum corresponds to the formation of Cu metal.

The narrow TPR peak of the aged precursor (Fig. 3) is in good agreement with the homogeneous microstructure of the corresponding single-phase Cu/ZnO catalyst [32]. The heterogeneous microstructure of the Cu/ZnO catalysts obtained from nonaged precipitates can already be inferred from the broad high-temperature TPR peak of the corresponding CuO/ZnO

precursor. The characteristic grouping of the CuO/ZnO precursors obtained from short-aged (0 and 15 min) and long-aged (30 and 120 min) precipitates clearly reflects the dominant influence of the aging procedure, not only on the structure of the precipitate, but also on the structure of the CuO/ZnO precursors (Figs. 1 and 2), the reduction behavior (Figs. 3 and 5), and, eventually, the resulting Cu/ZnO catalyst (Fig. 6). The CuO/ZnO precursors and the Cu/ZnO catalysts exhibit a "chemical memory" on the aging of the hydroxycarbonates during the first stages of preparation, and neither calcination nor reduction appears to erase the characteristic structural differences.

### 4.3. Correlations between copper structure and MSR activity

The crystalline hydroxycarbonate precipitates obtained after prolonged aging result in Cu/ZnO catalysts demonstrating a pronounced increase in MSR activity compared with the catalysts obtained from amorphous precipitates (Fig. 6). The Cu/ZnO catalysts obtained from long-aged precipitates exhibited a smaller copper crystallite size (Fig. 8b) and a larger copper surface area (Fig. 7a). Fig. 7b shows a nearly linear correlation between normalized activity of the catalysts and specific Cu surface area. Apparently, the specific copper surface area is the dominating factor for structure–activity correlations of Cu/ZnO catalysts. However, more evident examples of a nonlinear behavior of activity and Cu surface area have been shown recently [35], indicating that additional structural parameters govern the activity of the specific copper surface. The structural and catalytic properties of the Cu/ZnO materials studied confirm that in addition to the copper surface area, the increased microstrain in the nanostructured Cu particles as detected by XRD (Fig. 8a) and XAS (Fig. 11) correlates with the improved MSR activity of Cu/ZnO. Evaluation of various XRD lines in the patterns of the reduced Cu/ZnO catalysts revealed a strong anisotropy in Cu particle size and microstrain (Fig. 8). TEM images of the Cu/ZnO catalysts described here show a number of epitaxial relations between Cu and ZnO (e.g., Cu[111]||ZnO[110]), [32] which explains the anisotropic distribution of microstrain in the copper particles. The anisotropy in copper crystallite size appears to be more pronounced for the catalysts obtained from short-aged precipitates (Fig. 8), which is consistent with the heterogeneous microstructure of these materials. In addition to determining the microstrain in the copper nanoparticles by in situ XRD (Fig. 8) and EXAFS (Fig. 11), we could show that ex situ $^{63}$Cu nuclear magnetic resonance (NMR) spectroscopy investigations of the freshly reduced catalysts are in good agreement with the XRD results concerning the evolution of copper particle size and microstrain as a function of precipitate aging [17]. Moreover, tensile strain in the Cu nanoclusters was also reported by Wagner et al. based on Cu $L_{III}$-edge ELNES measurements of Cu/ZnO model catalysts [36]. However, with a combined change in crystallite size, composition (i.e., Zn content), and microstrain as a function of precipitate aging, the catalysts studied here are not suitable for unambiguously addressing the correlation between strain in copper and catalytic activity. Using other model systems, such as the recently reported thin Cu films on Si [37], it may be feasible to unravel the effect of strain on the electronic structure of Cu and thus on catalytic activity.

The correlation between microstrain in the copper nanoparticles (Fig. 8a) and catalytic properties (Fig. 6) clearly indicates that the improved interface between Cu and ZnO in the long-aged catalysts has a considerable influence on the microstructure of the Cu nanoparticles [32]. Moreover, it emphasizes the role of ZnO in determining the microstructure of the copper phase in addition to dispersing the copper particles and reducing sintering. The characteristic crystallization of the hydroxycarbonate precipitates during aging coincides with the increase in activity of the resulting Cu/ZnO catalysts (Fig. 6). TEM investigations have shown that calcination of the amorphous precipitates results in a heterogeneous microstructure with a majority of separated Cu and ZnO crystallites and hence a less active Cu/ZnO catalyst on reduction. Conversely, calcination and reduction of the crystalline precipitates obtained after aging have yielded catalysts in which Cu and ZnO are distributed in a homogeneous microstructure with small and disordered Cu crystallites having a distinct interface with ZnO [32].

In addition to the microstrain detected in the copper particles, the presence of Zn in both the CuO in the precursor and the Cu in the resulting catalyst emphasizes the defect-rich state of the "real" structure of the copper phase in Cu/ZnO catalysts (Fig. 11). The increase in the copper lattice constant (∼3.616 Å) and the distance of the first Cu shell (Fig. 12) of the Cu/ZnO catalysts obtained from short-aged precipitates indicates a larger amount of Zn in the copper phase compared with the Cu/ZnO catalysts obtained from long-aged precipitates (Fig. 11). $\alpha$-Brass (i.e., Cu Zn alloy) formation should occur only at temperatures above 580 K [3]. At a temperature of 523 K, the concentration of Zn in Cu amounts to about 1% Zn [38]. A higher oxygen vacancy concentration at the ZnO surface may increase the tendency of $\alpha$-brass formation in the copper bulk due to an enhanced diffusion rate through the Cu/ZnO interface and an improved miscibility of Cu and Zn in the real structure of the Cu/ZnO catalyst. It is more likely, however, that the formation of $\alpha$-brass during reduction at 523 K results from the presence of Zn in the CuO phase in the CuO/ZnO precursors (Figs. 1 and 2). It is evident from Fig. 11 that the amount of Zn in the copper nanoparticles exhibits a negative correlation with the microstrain in the copper phase and the performance of the Cu/ZnO catalysts (Fig. 6). Apparently, the presence of Zn in the copper particles is not the main source of the microstrain observed and is not required in the "real" structure of a more active Cu/ZnO catalyst.

### 4.4. Model of nanostructured Cu/ZnO catalysts as function of precipitate aging

The effect of precipitate aging on the microstructural properties of the resulting Cu/ZnO catalyst is schematically depicted in Fig. 13. The short-aged precipitates (0 and 15 min) exhibit on average larger Cu and ZnO particles on calcination and reduction (Fig. 8), which are more separated in these materials and have a reduced Cu/ZnO interface. Assuming that copper

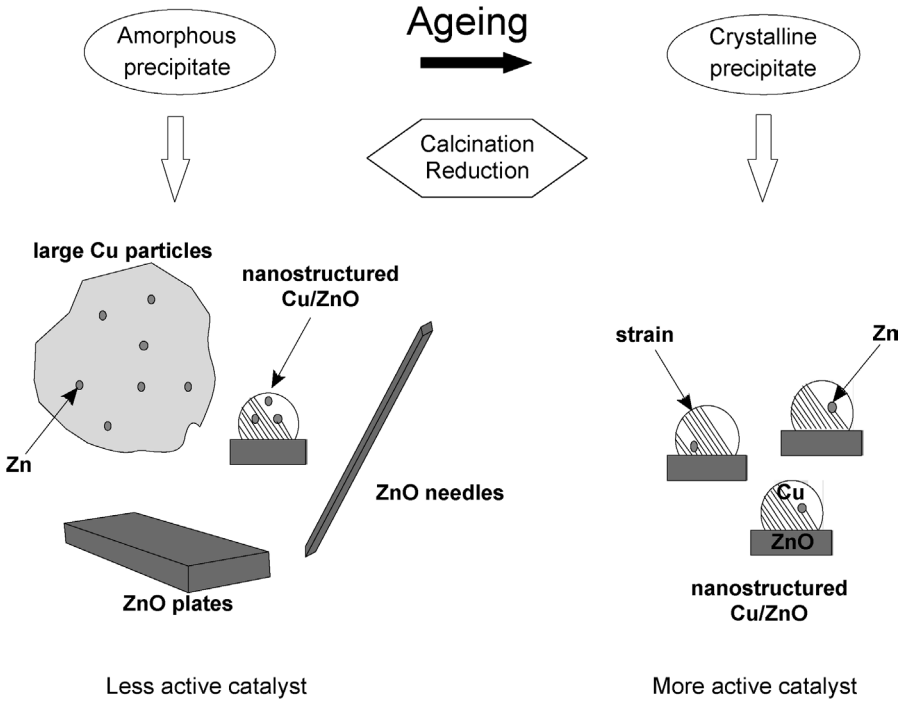


Fig. 13. Schematic model of the microstructural characteristics of Cu/ZnO catalysts obtained from differently aged precipitates (amorphous (<30 min), crystalline (>30 min)). Increasing ageing time leads to a more homogeneous microstructure, a decrease in average copper crystallite size of the Cu/ZnO catalysts, and an increase in the microstrain in the copper clusters because of the improved interface between Cu and ZnO. Additionally, increased precipitate ageing results in a decreased amount of Zn in Cu.

microstrain originates from an epitaxial orientation of copper on ZnO, the lower strain in the copper particles is indicative of this reduced Cu/ZnO interface. Hence less active Cu/ZnO catalysts obtained from short-aged precipitates exhibit a larger Cu crystallite size, a reduced interaction between Cu and ZnO, and a lower degree of microstrain in the copper crystallites.

Increasing the aging time of the precipitates (30 and 120 min) results in a more homogeneous microstructure of the resulting Cu/ZnO catalysts, which exhibits on average smaller Cu and ZnO crystallite sizes and higher copper surface areas. The improved interface between Cu and ZnO in these materials is indicated by the higher degree of microstrain in the copper crystallites. Apparently, the crystalline precipitates obtained after prolonged aging time have a well-defined distribution of Cu and Zn centers in the hydroxycarbonates. On calcination and reduction, this results in a reduced amount of Zn centers in both the calcined CuO/ZnO precursors and the reduced Cu/ZnO catalysts. Hence Cu/ZnO catalysts obtained from long-aged precipitates exhibit greater catalytic activity in methanol steam reforming, which correlates with a homogeneous microstructure, a smaller Cu crystallite size, a narrow crystallite size distribution, and a higher degree of microstrain.

Among the various methods described for the preparation of Cu/ZnO materials (e.g., impregnation, sol–gel synthesis, hydrothermal synthesis, chemical vapor deposition, mechanical milling) co-precipitation was found to be most suitable for preparing highly active Cu/ZnO catalysts [39]. Each precipitation parameter (i.e., pH, temperature, solvent, precipitation agent, additives, solution composition, and aging), as well as the posttreatment of the precipitates (i.e., washing, drying, calcination, and reduction), may affect the microstructure of the resulting Cu/ZnO catalyst. The work described in this paper indicates that the effect of precipitate aging on copper crystallite size and microstrain of the resulting Cu/ZnO catalyst can be readily adjusted through proper control of temperature and pH. However, the time of transition from an amorphous to a crystalline precipitate, and hence from a heterogeneous microstructure of a less active Cu/ZnO catalysts to a homogeneous microstructure of a more active catalysts, may depend on the amount of precipitate formed and may deviate from the ∼30 min time reported here.

## 5. Conclusions

We investigated the microstructural characteristics of the copper phase in Cu/ZnO catalysts for methanol steam reforming as a function of aging of the precipitated hydroxycarbonates during catalyst preparation. The structure–activity correlations presented here indicate that crystallinity, phase composition, and homogeneity of the resulting hydroxycarbonate strongly influence the microstructural properties of the final copper catalyst. Hence the structural characteristics of the precipitates as adjusted by an appropriate aging procedure govern the properties of the final catalyst (“chemical memory” effect). The schematic model proposed for the structural characteristics of the active Cu/ZnO catalyst as a function of precipitate aging emphasizes the defect-rich nature of the Cu and ZnO phases in the “real” structure of Cu/ZnO catalysts (“structural com-

plexity") and its implication for the catalytic activity in the steam reforming of methanol. Formation of a homogeneous microstructure with a similar chemical composition yielded a strong increase in catalytic activity. It emerges that microstructure design of improved heterogeneous catalysts must start at the very first stages of catalyst preparation, followed by optimizing the calcination and reduction conditions. Hence, in addition to studying structure–activity relationships of solid catalysts, the "chemical memory" of the material needs to be elucidated and considered in a rational catalyst design.

## Acknowledgments

The authors acknowledge grants from ZEIT-Stiftung ("Nanotechnology for the automobiles of the future") and Deutsche Forschungsgemeinschaft (SPP 1091, Bridging the gaps in heterogeneous catalysis") for generous financial support. They are grateful to Bettina Bems and Michael Schur for preparing the catalyst precursors and to Herry Purnama for catalyst screening. Robert Schlögl is gratefully acknowledged for his continuous support.

## References

[1] P.J. Wild, M.J.F.M. Verhaak, Catal. Today 60 (2000) 3.
[2] G.C. Chinchen, K.C. Waugh, Appl. Catal. 25 (1986) 101.
[3] Y. Knai, T. Wanatabe, T. Fujitani, M. Saito, J. Nakamura, T. Uchijama, Catal. Lett. 27 (1994) 67.
[4] J. Nakamura, I. Nakamura, T. Uchijama, Y. Kanai, T. Wanatabe, M. Saito, T. Fujitani, Catal. Lett. 31 (1995) 325.
[5] K. Klier, Adv. Catal. 31 (1982) 243.
[6] T. Fujitani, J. Nakamura, Appl. Catal. A 191 (2000) 111.
[7] B.S. Clausen, J. Schiøtz, L. Gråbæk, C.V. Ovesen, K.W. Jacobsen, J.K. Norskov, H. Topsøe, Top. Catal. (1994) 367.
[8] J.D. Grunwaldt, A.M. Molenbroek, N.-Y. Topsøe, H. Topsøe, B.S. Clausen, J. Catal. 194 (2000) 452.
[9] R. Burch, S.E. Golunski, J. Chem. Soc., Faraday Trans. 86 (1990) 2683.
[10] M.M. Günter, T. Ressler, B. Bems, C. Büscher, T. Genger, O. Hinrichsen, M. Muhler, R. Schlögl, Catal. Lett. 71 (2001) 37.
[11] M.M. Günter, T. Ressler, R.E. Jentoft, B. Bems, J. Catal. 203 (2001) 133.
[12] S. Sakong, A. Groß, Surf. Sci. 525 (2003) 107.
[13] D. Waller, D. Stirling, F.S. Stone, M.S. Spencer, Faraday Discuss. 87 (1989) 107.
[14] S.H. Taylor, G.J. Hutchings, A.A. Mirzaei, Catal. Today 84 (2003) 113.
[15] S.H. Taylor, G.J. Hutchings, A.A. Mirzaei, Chem. Commun. (1999) 1373.
[16] D.M. Whittle, A.A. Mirzaei, J.S.J. Hargreaves, R.W. Joyner, C.J. Kiely, S.H. Taylor, G.J. Hutchings, Phys. Chem. Chem. Phys. 4 (2002) 5915.
[17] B.L. Kniep, T. Ressler, A. Rabis, F. Steglich, M. Baenitz, F. Steglich, R. Schlögl, Angew. Chem. Int. Ed. 43 (2004) 112.
[18] B. Bems, M. Schur, A. Dassenoy, H. Junkes, D. Herein, R. Schlögl, Chem. Eur. J. 9 (2003) 2039.
[19] H. Purnama, T. Ressler, R.E. Jentoft, R. Schlögl, R. Schomäker, Appl. Catal. 259 (2004) 83.
[20] G.C. Chinchen, C.M. Hay, H.D. Vandervell, K.C. Waugh, J. Catal. 103 (1987) 79.
[21] O. Hinrichsen, T. Genger, M. Muhler, Chem. Ing. Tech. 72 (2000) 94.
[22] J.W. Ewans, M.S. Wainright, A.J. Bridgewater, D.J. Young, Appl. Catal. 7 (1983) 75.
[23] A. Szizybalski, F. Girgsdies, A. Rabis, Y. Wang, M. Niederberger, T. Ressler, J. Catal. 233 (2005) 297.
[24] J.I. Langford, J. Appl. Crystallogr. 11 (1978) 10.
[25] G.K. Williamson, W.H. Hall, Acta Metall. 1 (1953) 22.
[26] T. Ressler, J. Synch. Radiat. 5 (1998) 118.
[27] T. Ressler, J. Wong, J. Roos, I.L. Smith, Environ. Sci. Technol. 34 (2000) 950.
[28] A.L. Ankudinov, B. Ravel, J.J. Rehr, S.D. Conradson, Phys. Rev. B 58 (1998) 7565.
[29] D. Prabhakaran, A.T. Boothroyd, J. Cryst. Growth 250 (2003) 77.
[30] R.A. Brozi, S.J. Stewart, G. Punte, R.C. Mercader, R.D. Zysler, M. Tovar, Solid State Commun. 117 (2001) 311.
[31] B.S. Clausen, L. Gråbæk, H. Topsøe, L.B. Hansen, P. Stoltze, J.K. Nørskov, J. Catal. 141 (1993) 368.
[32] T. Ressler, B.L. Kniep, I. Kasatkin, R. Schlögl, Angew. Chem. Int. Ed. 44 (2005) 2.
[33] J. Sloczynski, R. Grabowski, A. Kozlowska, P.K. Olszewski, J. Stoch, Phys. Chem. Chem. Phys. 5 (2003) 4631.
[34] J.Y. Kim, J.A. Rodriguez, J.C. Hanson, A.I. Frenkel, P.L. Lee, J. Am. Chem. Soc. 125 (2003) 10684.
[35] M. Kurtz, H. Wilmer, T. Genger, O. Hinrichsen, M. Muhler, Catal. Lett. 86 (2003) 77.
[36] J.B. Wagner, P.L. Hansen, A.M. Molenbroek, H. Topsoe, B.S. Clausen, S. Helveg, J. Phys. Chem. B 107 (2003) 7753.
[37] F. Girgsdies, T. Ressler, U. Wild, T. Wübben, T.J. Balk, G. Dehm, L. Zhou, S. Günther, E. Arzt, R. Imbihl, R. Schlögl, Catal. Lett. 102 (2005) 91.
[38] M.S. Spencer, Surf. Sci. 192 (1987) 323.
[39] J.P. Shen, C. Song, Catal. Today 77 (2002) 89.